Cerebral Cortex, September 2019; 3796–3812

doi: 10.1093/cercor/bhy260
Advance Access Publication Date: 11 October 2018
Original Article

ORIGINAL ARTICLE

Sparse Representation in Awake Auditory Cortex: Cell-type Dependence, Synaptic Mechanisms, Developmental Emergence, and Modulation

Feixue Liang[1,2,3], Haifu Li[2,3], Xiao-lin Chou[2,3,4], Mu Zhou[2,4], Nicole K. Zhang[2], Zhongju Xiao[5], Ke K. Zhang[6], Huizhong W. Tao[2,3] and Li I. Zhang[2,3]

[1]Department of Medical Engineering, School of Biomedical Engineering, Southern Medical University, Guangzhou 510515, China, [2]Zilkha Neurogenetic Institute, Keck School of Medicine, University of Southern California, Los Angeles, CA 90033, USA, [3]Department of Physiology and Neuroscience, Keck School of Medicine, University of Southern California, Los Angeles, CA 90033, USA, [4]Neuroscience Graduate Program, University of Southern California, Los Angeles, CA 90089, USA, [5]Department of Physiology, School of Basic Medical Sciences, Southern Medical University, Guangzhou 510515, China and [6]Department of Pathology, the University of North Dakota, Grand Forks, ND 58202, USA

Address correspondence to F. Liang (liangfs@smu.edu.cn), H.W. Tao (htao@usc.edu) or L.I. Zhang (liizhang@usc.edu).

Abstract

Sparse representation is considered an important coding strategy for cortical processing in various sensory modalities. It remains unclear how cortical sparseness arises and is being regulated. Here, unbiased recordings from primary auditory cortex of awake adult mice revealed salient sparseness in layer (L)2/3, with a majority of excitatory neurons exhibiting no increased spiking in response to each of sound types tested. Sparse representation was not observed in parvalbumin (PV) inhibitory neurons. The nonresponding neurons did receive auditory-evoked synaptic inputs, marked by weaker excitation and lower excitation/inhibition (E/I) ratios than responding cells. Sparse representation arises during development in an experience-dependent manner, accompanied by differential changes of excitatory input strength and a transition from unimodal to bimodal distribution of E/I ratios. Sparseness level could be reduced by suppressing PV or L1 inhibitory neurons. Thus, sparse representation may be dynamically regulated via modulating E/I balance, optimizing cortical representation of the external sensory world.

Key words: cell attached recording, cortical inhibitory neuron, excitation/inhibition balance, developmental plasticity, Silent neuron, sparse coding

Introduction

It has been discovered in the past decades that only a small percentage of cortical neurons respond with spikes to a given sensory stimulus, with a vast majority of them being relatively silent (Hahnloser et al. 2002; Perez-Orive et al. 2002; Shoham et al. 2006; Hromadka et al. 2008; Poo and Isaacson 2009; Crochet et al. 2011; Epsztein et al. 2011; Barth and Poulet 2012; Kato et al. 2015). This dominant silence has often been

explained by a sparse coding strategy (Levy and Baxter 1996; Hahnloser et al. 2002; Perez-Orive et al. 2002; Laughlin and Sejnowski 2003; Olshausen and Field 2004; Barth and Poulet 2012; Petersen and Crochet 2013), that is, any specific sensory stimulus is selectively represented by a small subset of neurons and each neuron has its unique responding sensory space. Such strategy can allow a large information storage capacity while keeping a conservative energy budget (Levy and Baxter 1996; Laughlin and Sejnowski 2003; Olshausen and Field 2004).

Sparse cortical representation of sensory stimuli has been observed across several modalities, including somatosensory (Crochet et al. 2011), olfactory (Poo and Isaacson 2009), visual (Vinje and Gallant 2000), and auditory (Sutter et al. 1999; Hromadka et al. 2008; Chambers et al. 2014) cortices, in particular for supragranular neurons (Sakata and Harris 2009). In awake rodent primary auditory cortex (A1), recent calcium imaging studies have suggested that only about 20–30% of layer (L)2/3 neurons are excited by tone stimuli (Issa et al. 2014; Kato et al. 2015), although the actual percentage may be sensitively affected by the type of indicator used and its expression level.

Despite the well-documented phenomena of cortical sparse representation, there are outstanding questions remaining to be resolved. First, the underlying synaptic basis for sparse representation is not well understood. It is generally proposed that sensory response properties of cortical neurons are primarily determined by the interplay of excitatory and inhibitory synaptic inputs they receive (Isaacson and Scanziani 2011; Wu et al. 2011), and many previous studies have shown that cortical neurons ubiquitously receive inhibitory synaptic input (Sutter et al. 1999; Wehr and Zador 2003; Zhang et al. 2003; Liu et al. 2010, 2011). In the olfactory cortex of anesthetized mice, different odors nonselectively evoke strong inhibition in L2/3 pyramidal neurons, whereas the odor-evoked excitation is much less common (Poo and Isaacson 2009). In other words, cortical sparseness is at least partially inherited from excitatory input and may be enhanced by the global inhibition. In the barrel cortex of awake mice, examination of membrane potential changes of L2/3 pyramidal neurons in response to principle whisker–object contacts has revealed a commonly hyperpolarized reversal potential (i.e., more hyperpolarized than the spike threshold) for the evoked synaptic response (Crochet et al. 2011), suggesting that inhibitory input may play a critical role in controlling sparse spiking by "clamping" the membrane potential response in most of times below the spike threshold. The role of excitatory input in this case however has not been addressed. It is thus important to examine in the awake cortex both excitatory and inhibitory inputs to an individual neuron, which may regulate the sparse representation by acting together (Yu et al. 2014).

Second, previous studies on sparse representation have all been carried out in adult cortices. It remains unknown whether sparse representation is an intrinsic property of cortical circuits or if it arises during development in an activity-dependent manner. Given current understanding that functional properties of sensory cortical neurons undergo profound experience-dependent developmental changes (Zhang et al. 2001, 2002; Chang and Merzenich 2003; Yazaki-Sugiyama et al. 2009; Sun et al. 2010), we wonder if cortical sparseness is also subjected to developmental regulation and shaped by sensory experience.

Third, apart from a developmental regulation, it is unclear whether the sparseness level can be modulated acutely through manipulating some specific circuit components or input sources. The answer to this question may shed some light onto the functional significance of sparse representation.

In this study, we established stable cell-attached recording techniques in awake auditory cortex of both adult and young mice. By cross-examining neuronal responsiveness to a variety of sound types in the primary auditory cortex (A1), we found that tones and noise were 2 fundamental sound categories that could be used to evaluate a lower bound of cortical sparseness. Using these sounds, we examined cell type and laminar differences of sparse representation and revealed that sparse representation was salient in the L2/3 excitatory neuron population. Using sequential cell-attached and whole-cell voltage clamp recordings, we compared excitatory and inhibitory inputs between responding and nonresponding neurons and found that the nonresponsiveness could be explained by relatively weaker excitation and lower E/I ratios. Furthermore, we discovered that sparse representation in fact emerged during development in a sensory experience-dependent manner, and that this process was accompanied by differential changes of excitatory input strength and a transition from unimodal to bimodal distribution of E/I ratios. Finally, we found that the sparseness level was subjected to modifications by manipulating activity of cortical parvalbumin (PV) or L1 inhibitory neurons. These developmental and functional modulations of cortical sparseness may allow auditory cortex to extend its functional spectrum during adaptive changes.

Materials and Methods

All experimental procedures used in this study were approved by the Animal Care and Use Committee at the University of Southern California.

Animal Preparation for Recordings

For adult animals, C57BL/6 J mice of either sex aged 2–3 months were used. Each animal was first tested with multiunit recordings to map the frequency representation in the auditory cortex. Auditory response thresholds were found normal for the examined frequency range (2-64 kHz) for all the animals used in this study. Animals for awake recordings were prepared in a similar way as previously described (Zhou et al. 2014; Xiong et al. 2015; Zhang et al. 2018). Mice were housed with a 12-h light/dark cycle. 3–7 days before the recording, the animal was anesthetized with isoflurane (1.5%, v/v) and a screw for head fixation was mounted on the top of the skull with dental cement. Skull over the A1 was cleaned and protected from being covered by dental cement. During the recovery period, the mouse was trained to get accustomed to the head fixation on the recording setup. To fix the head, the screw was tightly clamped by a custom-made post holder. The head-fixed animal was able to run freely on a flat rotatable plate mounted on an optical shaft encoder (US Digital). For recording, the mouse was briefly anesthetized with isoflurane to perform a small craniotomy (~0.8 × 0.8 mm^2) over the A1 one day before the experiments. The craniotomy was properly covered with silicon elastomer (Kwik-CAST, WPI) and sealed until recording. Recording experiments were carried out in a sound-attenuation booth (Acoustic Systems), only in animals which exhibited smooth running on the plate. They spent about 10%-20% of time running. Each recording session lasted for about 4 h. The animal was given drops of 5% sucrose (w/v) through a pipette every hour. Between sessions, animals were returned to the home cage for a > 1-h break. For young animals, C57BL/6 J mice of either sex older than P16 (developmental stage 1, ST1, P18–P21; ST2, P25–P28; ST3, P32–P35) were used. 2–3 days before the recording, the mouse was anesthetized with isoflurane (1.5%, v/v) in order to mount a post on the skull.

For recordings, sound stimuli were delivered in one setup through a closed acoustic delivery system with a TDT EC1 coupler speaker (calibrated to generate flat outputs from 2 kHz to 64 kHz) connected with the left ear and in another through a calibrated open field speaker (XT25G30-04 1'' Dual Ring Tweeter; Vifa) positioned 10 cm from the mouse head facing the left ear, for TRFs and sounds within 2–32 kHz. Multiunit recordings were first made with a tungsten electrode (2 MΩ, FHC) to determine the CF for an array of recording sites. The A1 was identified based on the tonotopic gradient of CFs as well as the response properties, as described in previous studies (Hackett et al. 2011; Guo et al. 2012; Li et al. 2014, 2015; Zhou et al. 2014). The animal head was tilted so that the electrode could penetrate the A1 surface at an angle of about 80°.

In vivo cell-attached and whole-cell recordings

Patch recordings were made with an Axopatch 200B amplifier (Molecular Devices). The patch pipette, controlled by a micromanipulator (Siskiyou), was lowered into the A1 at the same angle as in multiunit recordings. The cortical surface was covered with 3.5% agar prepared in warm artificial cerebrospinal fluid (ACSF; 124 mM NaCl, 1.2 mM NaH_2PO4, 2.5 mM KCl, 25 mM $NaHCO_3$, 20 mM glucose, 2 mM $CaCl_2$, 1 mM $MgCl_2$). For loose-patch (with 100–500-MΩ seal) recording from excitatory neurons, patch pipette (resistance of 5–7 MΩ) was filled with ACSF. Pipette capacitance was fully compensated. Signals were recorded in voltage clamp mode at 20 kHz sampling rate, with a command voltage applied to adjust the baseline current to be zero. If a cell did not exhibit spontaneous spikes within 10 min, it was not further recorded.

For whole-cell current clamp recordings, patch pipette contained a potassium-based solution: 130 mM potassium gluconate, 4 mM MgATP, 0.3 mM GTP, 8 mM phosphocreatine, 10 mM HEPES, 10 mM EGTA, 5 mM KCl, 1 mM $CaCl_2$, 1% biocytin (*w/v*), pH = 7.3. Membrane potentials were recorded under current clamp mode. Signals were low-pass filtered at 5 kHz and sampled at 20 kHz. Input resistance was measured by injecting a negative pulse current (–50 or –100 pA) to the cell. For whole-cell voltage clamp recordings, patch pipette (resistance of 4–5 MΩ) contained a cesium-based solution: 125 mM cesium gluconate, 5 mM TEA-Cl, 4 mM MgATP, 0.3 mM GTP, 10 mM phosphocreatine, 10 mM HEPES, 10 mM EGTA, 2 mM CsCl, 1.5 mM QX-314, 1% biocytin (*w/v*), pH = 7.3. Sequential cell-attached and whole-cell recordings were applied as previously described (Poo and Isaacson 2009; Sun et al. 2010). The sound-evoked and spontaneous spikes of the patched neuron were first recorded before breaking in the membrane to determine its spike response properties. A cell was not further recorded if it did not exhibit spontaneous spikes within 10 min. After forming a whole cell, whole-cell capacitance was fully compensated and the initial series resistance (Rs, 15–50 MΩ) was compensated for 40–50% to achieve an effective Rs of 10–30 MΩ. Signals were low-pass filtered at 2 kHz and sampled at 10 kHz. Only cells with resting membrane potential lower than –55 mV were studied. A –10 mV junction potential was corrected. Excitatory and inhibitory synaptic currents were recorded by clamping the cell at –70 and 0 mV, respectively. Although the linear I–V relationship (Fig. 3*K*) for recorded currents supported a reasonably good clamping quality, potential errors caused by imperfect space clamp should be carefully considered.

The success rate of the recordings was largely improved over our previous studies. On average, 2–4 good whole-cell recordings (maintained for 20–40 min) or more than 20 loose-patch recordings were obtained in each animal. The recording sites in relation to the tonotopic gradient of A1 were marked. The laminar locations of the recorded neurons were determined based on the micromanipulator reading, and in some cases confirmed by post hoc reconstruction (see Supplementary Fig. S3*F–H*). We found a relatively good correspondence between the traveling depth of the recording pipette from the pia and the reconstructed laminar location of the recorded neuron ($\Delta D = -6.1 \pm 26.9$ μm, mean ± SD, Supplementary Fig. S3*H*). The L2/3 neurons were sampled at a cortical depth of 175–325 μm from the pial surface, L4 neurons at a depth of 350–500 μm (Li et al. 2014; Zhou et al. 2014). As demonstrated previously (Liu et al. 2010; Sun et al. 2010; Li et al. 2014) and post hoc reconstruction (Fig. S3*F,G*), the blind whole-cell recording method with relatively large pipette openings resulted in almost exclusive sampling from excitatory cortical neurons.

Optogenetically Guided Loose-Patch Recordings from PV Neurons

We expressed ChR2 in PV neurons by 2 ways. The first was through viral delivery (Li et al. 2013, 2014). Adult PV-Cre (Jackson Laboratory) mice were anesthetized with 1.5% isoflurane. A small cut was made on the skin covering the right A1 and the muscles were removed. Two ~0.2-mm craniotomies were made in the A1 region (temporal lobe, 2.7 and 3.2 mm caudal to Bregma). Adeno-associated viruses (AAVs) encoding Cre-dependent ChR2 were purchased from the University of Pennsylvania Viral Vector Core: AAV2/9.EF1α.DIO.hChR2 (H134R)-EYFP.WPRE.hGH (Addgene 20 298). The virus was delivered using a beveled glass micropipette (tip diameter, ~40 μm) attached to a microsyringe pump (World Precision Instruments). Injections were performed at 2 locations and 2 depths (300 and 600 μm), at a volume of 100 nl per injection and at a rate of 20 nl min^{-1}. After each injection, the pipette was allowed to rest for 4 min before withdrawal. We then sutured the scalp, injected buprenorphine at 0.1 mg per kg and returned the mouse to its home cage. Mice were allowed to recover for 3–4 weeks. The second way was to cross the PV-Cre mice with the floxed ChR2 mouse line (#012 567, The Jackson Laboratory). The genotypes were identified by genotyping, and 2-month-old mice of correct genotypes were used.

On the day of recording, loose-patch recordings using pipettes of smaller tip openings (resistance of ~10 MΩ) (Li et al. 2013; Zhou et al. 2014) were performed. An optic fiber connecting to a blue LED source (470 nm, Thorlabs) was positioned close to the cortical surface of the recording site. We actively searched for neurons exhibiting LED-evoked spikes with loose-patch recording paradigm, which were identified as PV neurons. After each experiment, that brain was sectioned and imaged to further confirm the expression of ChR2-EYFP. Because of results shown in Fig. 2*C*, neurons exhibiting narrow spikes (trough-peak interval <0.3 ms) recorded in non-ChR2-expressing animals were also identified as PV neurons.

Optogenetically Suppressing Inhibitory Neurons

For suppressing PV neurons, AAV1-CAG-FLEX-ArchT-GFP (Addgene 28 307, from UNC vector core) was injected into A1 of PV-Cre mice similarly as described above. Green LED light (530 nm, 500-ms duration) was paired with tones/noise in an interleaved manner. For suppressing L1 neurons, the viral vector was locally injected into GAD2-Cre mice (Jackson

Laboratory) via iontophoresis using 3 μA currents for 5 s, at a depth of 50 μm and at 4 different sites within A1. Animals were examined postrecording to confirm that ArchT-GFP expression was limited within L1.

Sound Generation

Software for sound stimulation and data acquisition was custom-developed in LabVIEW (National Instruments). Sound stimuli of various types (Wang et al. 2005; Chambers et al. 2014) were generated as shown in Supplementary Fig. S2. Except for TRF mapping, each individual stimulus was repeated for 10–20 times. Stimuli include pure tones (2–64 kHz spaced at 0.1 octave, 50-ms duration, 3-ms ramp, 0–70 dB sound pressure level (SPL) spaced at 10 dB, in pseudorandom sequence, 3 repetitions, 0.5-s interstimulus interval), noise (broadband white noise, 50-ms duration, 3-ms ramp, 30 and 60 dB SPL,10–20 repetitions), band noise (0.5 or 1 octave width centering on the CF of the recording site), frequency-modulated (FM) sweeps (frequency logarithmically changing from 0.5 to 64 kHz or from 64 to 0.5 kHz for broad-range FM sweeps, or ±0.5 octave centered on the CF of the recording site for narrow-range FM sweeps, at a speed of 14, 20, 35, 70, 140, 280, and 700 octave/s, 30 and 60 dB SPL, in pseudorandom sequence, 10 repetitions, 2-s interstimulus interval), click sound (30 and 60 dB SPL, 10 repetitions, 2-s interstimulus interval), amplitude-modulated (AM) sound (CF tone or noise carrier, sinusoidal modulation of intensity at 2, 4, 8, 16 Hz, 30 and 60 dB SPL maximum intensity, 1-s duration, 10 repetitions, modulation index at 100%, 2-s interstimulus interval), trains of CF tones and noise (30 and 60 dB SPL intensity, 1-s duration, with repetition rate at 4, 8, 16, 32, and 64 Hz, 10 repetitions, 2-s interstimulus interval), a cat's "meow" sound (16-s duration, 10–20 repetitions, 20-s interstimulus interval), and modified jungle sound (to be fit into mouse hearing range, 10–20 repetitions, 12-s duration, 16-s interstimulus interval). Note that for any recorded neuron, frequency components of the testing sound stimuli covered the expected CF of the recorded cortical site (determined during the pre-mapping). For tone-responsive neurons, the best intensity (intensity at which strongest spike responses were evoked) was identified online, and tones at this intensity (or maximum intensity used) were applied to measure intracellular responses (5 repetitions). Best frequency was defined as the frequency that evoked the strongest response at a given intensity. For many experiments determining the sparseness level in a cortical layer, we only tested noise/tone responses in each cell, which took about 5–10 min.

Noise Rearing

Litters of mouse pups together with their mothers were housed in a sound-attenuation chamber with 12-h light/12 h dark cycles. They were exposed to continuous white noise, which was applied during the dark cycles, from P9 to P35, as previously described (Zhang et al. 2002; Chang and Merzenich 2003; Kim et al. 2013). The white noise was produced with a LabView program and delivered through an open field speaker. The intensity was gradually increased to 60 dB SPL over the first 3 days. Mice had normal access to food and water in the chamber. Their weights and behaviors were monitored.

Data Analysis

We performed data analysis with custom-developed software (MATLAB, MathWorks). Analysis performers were partially blind to the conditions of the experiments, as the data from all the recorded neurons were first pooled together for a randomized batch processing without categorizing the neurons according to their specific identity (e.g., age, condition, laminar location, etc.).

Sound-evoked Spike Responses

In cell-attached recordings, spikes could be detected without ambiguity because their amplitudes were normally higher than 50 pA, whereas the baseline fluctuation was <5 pA. The onset latency of tone-evoked spike responses was determined from the peri-stimulus spike time histogram (PSTH) generated from responses to all the tones as the lag between the stimulus onset and the time point at which spike rate exceeded the average spontaneous firing rate by 2 standard deviations of baseline fluctuations. To categorize a neuron into R or NR type, we calculated z-scores. For transient stimuli such as tones and noise, firing rate within the 100-ms analysis window after the stimulus onset was calculated. The cell was considered as an R cell if the firing rate exceeded the spontaneous firing rate by 2 standard deviations of baseline fluctuations (i.e., z-score > 2). For longer stimuli such as FM sweeps and natural sounds, we calculated time-dependent firing rates using a 100-ms sliding window starting from the onset of the stimulus and sliding through the entire duration of the stimulus. As long as firing rate at any time point exceeded the spontaneous firing rate by 2 standard deviations of baseline fluctuations, the cell was considered as an R cell. Otherwise, a cell was considered as a NR cell.

Synaptic Responses

Synaptic response traces evoked by the same stimulus were averaged. Synaptic onset latency was determined at the time point where the evoked current exceeded the average baseline by 2 standard deviations. Peak amplitude was determined by averaging within a 5-ms window centered on the response peak after subtracting the baseline current. Excitatory and inhibitory synaptic conductances were derived according to $\Delta I = G_e^*(V - E_e) + G_i^*(V - E_i)$ (Borg-Graham et al. 1998; Sun et al. 2010; Li et al. 2013, 2014; Xiong et al. 2013; Zhou et al. 2014). ΔI is the amplitude of the synaptic current at any time point after subtracting the average baseline current; G_e and G_i are the excitatory and inhibitory synaptic conductance; V is the holding voltage, and E_e (0 mV) and E_i (–70 mV) are the reversal potentials. The clamping voltage V was corrected from the applied holding voltage (V_h): $V = V_h - Rs^*I$, where Rs is the effective series resistance. By holding the recorded cell at 2 different voltages (the reversal potentials for excitatory and inhibitory current, respectively), G_e and G_i could be resolved from the equation. Resting conductance was calculated based on the average baseline currents within a 50-ms window before the onset of evoked currents recorded under 2 different voltages (–70 and 0 mV).

Derive Postsynaptic Potential Responses

We used a conductance-based Neuron model to simulate the membrane potential response by integrating experimentally observed excitation and inhibition (Xiong et al. 2013; Li et al. 2014):

$$V_{t+1} = -\frac{dt}{C}[G_{e_t}(V_t - E_e) + G_{i_t}(V_t - E_i) + G_r(V_t - V_{rest})] + V_t$$

The values of C (100 pF) and G_r (resting conductance, 5 nS, measured from the baseline currents at different holding

potentials) were based on the mean measurement values for adult neurons. The resting membrane potential (V_{rest}) was –65 mV. The same parameters were used when deriving postsynaptic potential (PSP) responses for young neurons.

Statistical Test

Shapiro–Wilk test was first applied to exam whether samples had a normal distribution. In the case of a normal distribution, *t*-test or ANOVA test was applied. Otherwise, a nonparametric test (Wilcoxon signed-rank test) was applied. Data were presented as mean ± SD if not otherwise specified. To test bimodality of E/I ratio distribution, Shapiro–Wilk normality test first showed that data from ST1 mice could fit a normal distribution ($P = 0.62$), whereas data from adult mice were not normally distributed ($P = 0.00066$). Since adult data (Fig. 5*D*) appeared to have 2 peaks, we attempted to fit a mixture Gaussian distribution using EM algorithm. The resulting model was formed by the sum of 2 normal distributions with the means of 0.429 and 1.040, respectively. Their standard deviations were the same, 0.145. The first normal distribution represented 74.5% of the population and the second represented the remaining 25.5%. We then performed goodness-of-fit test for fitting the mixture Gaussian model to the young and adult data. The adult data adequately fit into the mixture model ($P = 0.97$), while the ST1 data failed ($P = 0.0013$). Therefore, the adult E/I ratios formed a 2-mode mixture Gaussian distribution, while the ST1 E/I ratios formed a single-mode normal distribution.

Results

Sparse Representation in Layer 2/3 of Awake Mouse A1

In A1 of awake adult mice (Fig. 1*A*), we examined neuronal responsiveness with *in vivo* cell-attached loose-patch recording (Zhou et al. 2014), which is a relatively unbiased recording method regardless of low- or high-spiking neurons (Hromadka et al. 2008; Barth and Poulet 2012; Zhou et al. 2014). With stable long-term recordings (Fig. 1*B* and Supplementary Fig. S1*A–C*), we were able to characterize spike responses of putative excitatory neurons in L2/3 to a variety of auditory stimuli that covered several fundamental sound categories (Supplementary Fig. S2). A1 neurons responded in 3 different ways based on the presence or absence of spike rate increases. The example neuron 1 responded to pure tones of varying frequency and intensity (Fig. 1*C*). In the frequency–intensity space, a tonal receptive field (TRF) could be identified, from which the characteristic frequency (CF, defined as the frequency that evokes spiking responses at the lowest intensity) of the cell could be determined (Fig. 1*C*). The neuron also exhibited responses to FM sweeps, the magnitude and timing of which were modulated by the direction and speed of the sweeps (Fig. 1*D*). Additionally, it responded to white noise (Fig. 1*E*), AM noise (Fig. 1*F*), as well as natural sounds such as a cat's meow (Fig. 1*G*) and jungle sounds (Supplementary Fig. S1*D*). In short, this neuron could respond to almost all the sound categories tested, while being selective for sound frequency. The example neuron 2 did not exhibit clear responses to tones or an identifiable TRF (Fig. 1*H*), or responses to FM sweeps (Fig. 1*I*), but it did respond to noise (Fig. 1*J*), AM noise (Fig. 1*K*), as well as a cat's meow (Fig. 1*L*) and jungle sounds (Supplementary Fig. S1*E*). For the example neuron 3, no tone-evoked response or TRF was clearly identified (Fig. 1*M*), nor any response evoked by FM sweeps, noise, AM noise, or natural sounds (Fig. 1*N–Q* and Supplementary Fig. S1*F*). That is, it did not respond to any sound category tested.

We have recorded from a total of 310 putative excitatory neurons in L2/3 (see Materials and Methods) and subjected them to as many sound categories as possible. We found a large overlap of responsiveness between noise/tone and other sound categories (Fig. 1*R*). 22% (67 out of 310, red portion) of the recorded neurons were excited by tones, and nearly all of them (97%, 65 out of 67) were also excited by noise. 100% of tone-driven neurons were also excited by FM sweeps (both broad- and narrow-range sweeps), as well as trains of CF tones and AM CF tones. Conversely, 100% of neurons responding to FM sweeps, to a train of tone pips or AM tones (corresponding to the CF of the recorded site), were also excited by single-tone pips. 62% of tone-driven neurons also responded to a click sound, while 100% of click-responsive neurons responded to pure tones. While nearly all tone-driven neurons (97%) were also excited by noise, only 61% of noise-driven neurons (Fig. 1*R*, blue portion) responded to tones. The remaining 39% of noise-driven neurons thus responded similarly as the example neuron 2. 100% of neurons responding to white noise also responded to narrow-band (NB) noise (centered on the CF of the recording site), to trains of noise and AM noise, as well as to natural sounds. Conversely, all neurons responding to the latter variety of stimuli were also responsive to broadband noise. 54% of noise-driven neurons also responded to a click sound, while 100% of click-responsive neurons responded to noise. Tone- or noise-responding ("R") neurons together accounted for 35% of the L2/3 excitatory neuron population (Fig. 1*R*). The rest of the population (65%, white portion) were not excited by any sound category tested. In some of these cells (about 10% of the population), we observed that noise or tones suppressed the spontaneous firing rate (Supplementary Fig. S1*G*), reminiscent of a previous Ca^{2+} imaging study (Kato et al. 2015). The suppression was delayed relative to the spiking responses of R cells (Supplementary Fig. S1*H*). It is worth noting that this type of neuron was considered as nonresponding ("NR"). In this study, sparseness means that the percentage of R neurons under a specific type of sound stimulus is low. That is, the lower the percentage of R neurons, the higher the sparseness level. Because noise/tone-responsiveness covers many more complex sounds, noise and tones were utilized in our later experiments to evaluate a lower bound of cortical sparseness. The sparseness examined in this study is equivalent to "population sparseness" specified in several previous studies (Vinje and Gallant 2000; Willmore and Tolhurst 2001; Chambers et al. 2014; Kato et al. 2015).

Laminar Dependence of Cortical Sparseness

Based on the responsiveness to tones and noise, we examined sparseness at different laminar stages of cortical processing. In this study, R and NR cells were defined by a statistical assessment of evoked firing rate (FR): if a cell's evoked FR under any testing stimulus at any time during the analysis window exceeded the average spontaneous FR by 2 standard deviations of baseline activity (i.e., z-score > 2), it was defined as an R cell; otherwise it was defined as an NR cell (Fig. 1*S*). R and NR cells did not differ in the level of spontaneous FR (Fig. 1*T*). Among different cortical layers, L2/3 had the highest level of sparseness, as shown by the lowest percentage of R cells (Fig. 1*U*), while other layers had a similar level of sparseness which was lower than that in L2/3 (Fig. 1*U*). Therefore, sparseness level was particularly enhanced in L2/3, the principal output layer to other cortical areas (Petersen and Crochet 2013). Within L2/3, a similar level of sparseness was observed across different frequency bands of A1 (Fig. 1*V*).

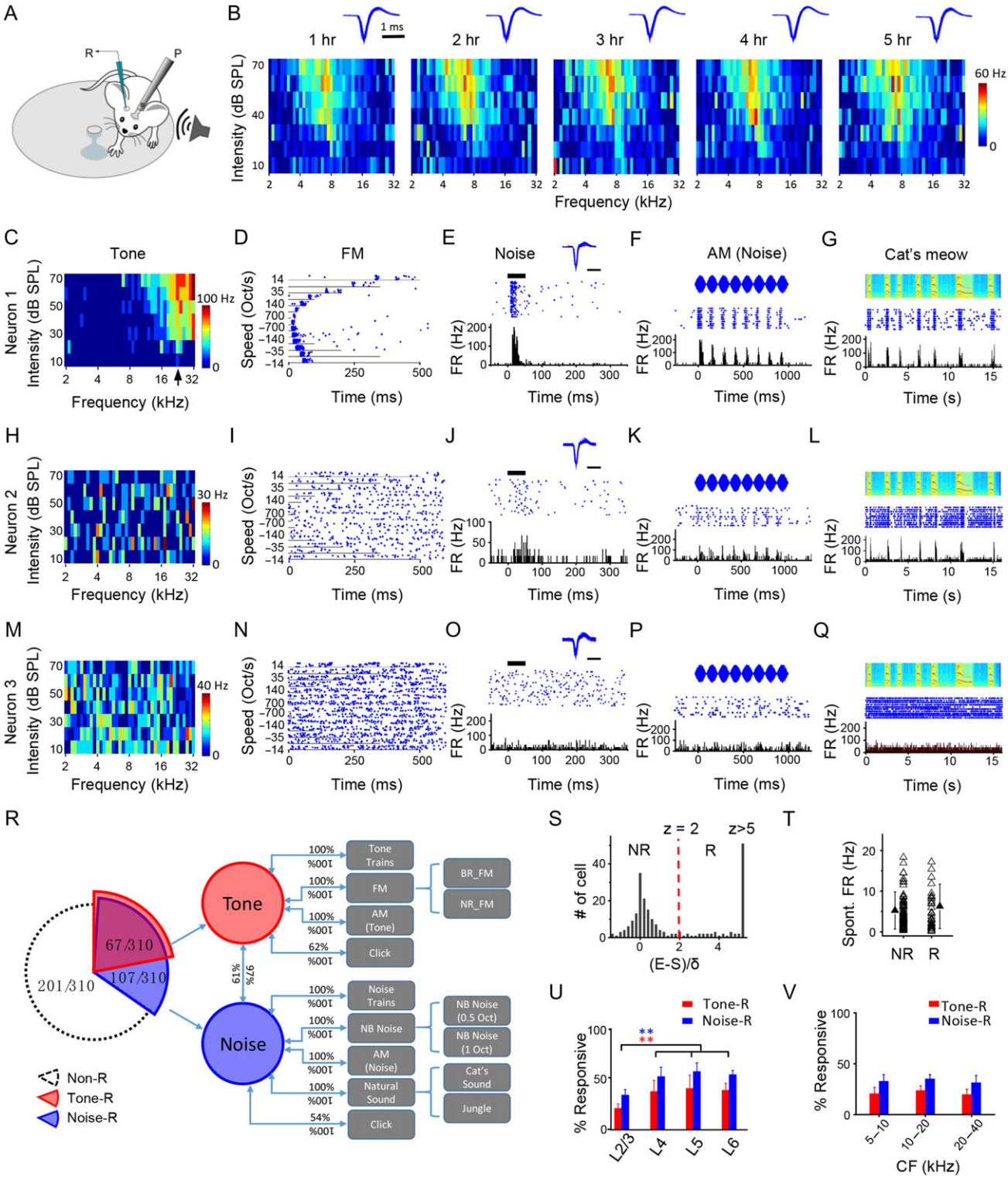

Figure 1. Response sparseness in L2/3 of A1 in awake adult mice revealed by loose-patch recording. (*A*) Experimental setup. The mouse was head-fixed and allowed to run on a rotatable plate. Sound was applied to the contralateral ear. R, recording pipette; P, post for head fixation. (*B*) Color maps show frequency–intensity TRFs of a neuron measured at different recording times. Color displays the firing rate evoked by each tone. Note the consistency of TRFs over time. Inset, superimposed 100 randomly selected spike waveforms at the corresponding time. (*C*) TRF of an example neuron (neuron 1). Arrow points to the CF of the neuron. (*D*) Raster plot of spikes to FM sweeps at different speeds and directions (positive values indicate sweeping from low to high frequencies) of the same neuron in (*A*). (*E*) Raster plot (top) and PSTH (bottom) for spike responses of the same neuron to a pulse of white noise (50-ms duration, marked by the thick line). Inset, superimposed 100 individual spikes. Scale: 1 ms. (*F*) Raster plot (middle) and PSTH (bottom) for spike responses of the same neuron to AM noise. Top, waveform for the intensity modulation. (*G*) Raster plot (middle) and PSTH (bottom) for responses of the same neuron to a cat's meow sound. Top, spectrogram for the sound. (*H–L*) Responses of another example neuron (neuron 2) to different sound categories. Data displays are similar as in (*C–G*). (*M–Q*) Responses of another example neuron (neuron 3). (*R*) Cross-examination of responsiveness to different sound categories. BR: broad range; NR: narrow range; NB: narrow band. (*S*) Distribution of *z*-scores in the recorded population.

Sparse Representation is Not Observed for PV Inhibitory Neurons

We next examined whether the sparseness observed for L2/3 excitatory cells could apply to inhibitory neurons. We focused on PV neurons, one of the major inhibitory cell subtypes (Rudy et al. 2011). By injecting AAV encoding Cre-dependent channelrhodopsin2 (ChR2) (Fenno et al. 2011) into PV-Cre mice (Fig. 2A), we were able to identify PV neurons with loose-patch recording (see Materials and Methods) based on their spike responses to pulses of blue LED light applied to the A1 surface (Fig. 2B). LED light evoked spikes in ChR2-expressing PV neurons with a latency of 2.1 ± 0.4 ms (mean ± SD, n = 150 spikes in 15 cells). The PV neurons exhibited narrower spike waveforms as compared with putative excitatory neurons (Fig. 2C), consistent with our previous reports (Zhou et al. 2014; Li et al. 2015). We found that the high-level cortical sparseness observed in the excitatory cell population was absent in the PV cell population: approximately 96% of the recorded PV cells were excited by tones or noise (Fig. 2D) when we used a similar criterion to differentiate NR versus R cells for this type of neuron (Fig. 2F). TRFs and temporal response patterns of example PV cells are shown in Fig. 2E. Their TRFs were noticeably broad, consistent with our previous observations (Li et al. 2015). In general, PV cells had a higher spontaneous FR (Fig. 2G), higher evoked FR (Fig. 2H), and broader TRF (Fig. 2I) than putative excitatory cells. They also tended to have a lower intensity threshold than excitatory cells (Fig. 2J). These properties indicate that PV inhibitory neurons exhibit higher responsiveness (Ma et al. 2010; Hofer et al. 2011; Li et al. 2015) and much lower population sparseness than excitatory cells.

Sparse Representation is Absent at the Subthreshold Level

What are the mechanisms for sparse representation? By performing sequential cell-attached and whole-cell recordings from the same cells (see Materials and Methods), we first examined if the apparent cortical sparseness was due to a lack of auditory-evoked input to many neurons. We focused on the tone-responsiveness to gain a general understanding. After patching onto the cell membrane and before breaking in to form a whole cell, we recorded spikes of the cell to tones used for measuring TRFs. Fig. 3A,B illustrates representative tone-responding and nonresponding neurons, respectively. Their spike responses to individual tones at a relatively high intensity (left top panel) and the PSTH generated from these responses (right panel) are shown. Afterward in whole-cell current clamp mode (with a K^+-based internal solution used), we recorded their membrane potential (V_m) responses (left bottom panel). The NR neuron exhibited depolarizing V_m responses to a broad range of tone frequencies similar to the R cell, although none of these V_m responses produced a spike. In a total of 26 similarly recorded L2/3 neurons, we identified 20 NR and 6 R cells. All these neurons exhibited tone-evoked depolarizing PSP responses (Fig. 3C), indicating that they all received synaptic inputs. Sparse representation was thus absent at the synaptic input level, consistent with a previous study (Crochet et al. 2011). The R cells exhibited a significantly stronger depolarization evoked by the best tone (defined by the frequency that evokes the strongest response at the best or maximum intensity tested) than the NR cells (R: 30.6 ± 1.01 mV; NR: 19.0 ± 5.91 mV; $P < 0.001$, t-test, Fig. 3C). A similar conclusion could be made when noise-responding and -nonresponding cells were compared (Supplementary Fig. S3A,B). On the other hand, the R and NR cells did not differ in the level of resting membrane potential, input resistance or spike threshold (Supplementary Fig. S3C–E). Nor did they appear to be different in dendritic morphology or cortical depth (Supplementary Fig. S3F–H). Our data thus indicate that the differential responsiveness of R and NR cells is likely attributed to different levels of synaptic input they receive.

Synaptic Mechanisms Underlying Sparse Representation

We next examined excitatory and inhibitory synaptic mechanisms underlying the differential responsiveness of R and NR cells, with sequential cell-attached and whole-cell voltage clamp recordings from the same cells in L2/3 using a Cs^+-based internal solution (see Materials and Methods). Again, R and NR cells were identified based on their spike responses to tones or noise recorded before forming the whole cell (Fig. 3D,E, left panel). Afterward in whole-cell voltage clamp mode, we recorded excitatory synaptic currents by clamping the cell's membrane potential at −70 mV, and inhibitory synaptic currents at 0 mV (Fig. 3D,E, right panel). Similar to our previous observation (Zhou et al. 2014), the peak amplitude of excitation was linearly correlated with that of inhibition evoked by the same stimulus, with the slope of the linear regression line reflecting an overall E/I ratio (Fig. 3F). Comparing the representative R (Fig. 3D) and NR (Fig. 3E) cell, a noticeable difference is that E/I ratio was lower in the NR cell (Fig. 3F). In addition, the excitatory input appeared weaker in the NR cell (Fig. 3G).

Excitation and inhibition were examined in 34 NR and 11 R cells identified based on tone-responsiveness. In the NR cells, tone-evoked excitation was significantly weaker than inhibition in terms of peak amplitude ($P < 0.001$, Wilcoxon signed-rank test), while in the R cells excitation and inhibition had similar amplitudes ($P > 0.05$, Wilcoxon signed-rank test) (Fig. 3H). The NR cells exhibited weaker excitation than the R cells ($P < 0.001$, Wilcoxon signed-rank test), whereas the strength of inhibition did not differ between the NR and R cells ($P > 0.05$, Wilcoxon signed-rank test) (Fig. 3H). The resulting E/I ratio thus appeared to be a good parameter for separating NR and R groups (Fig. 3I), with the NR cells having significantly lower E/I ratios than the R cells (NR: 0.43 ± 0.15; R: 1.04 ± 0.19; $P < 0.001$, t-test). Similar conclusions could also be made when the total charge of synaptic current was analyzed (Supplementary Fig. S4A–C) or when noise-evoked synaptic responses were compared (Supplementary Fig. S4D–F). As for temporal properties of the synaptic responses, NR and R cells did not differ in the onset latency of either excitation or inhibition (Fig. 3J), in the rising time of synaptic dynamics for either excitation or inhibition (Supplementary Fig. S4G), or in the time interval between peak excitation and peak inhibition (Supplementary Fig. S4H), again supporting the notion that these 2 groups of cells are unlikely to arise from different synaptic circuits.

E, maximally evoked firing rate; S, spontaneous firing rate; δ, standard deviation of baseline activity. A cell with z-score ≤2 is defined as a nonresponding (NR) cell. Otherwise a cell is defined as a responding (R) cell. Cells with z-score >5 are grouped together. (T) Comparison of spontaneous firing rate (FR) between the NR and R groups. There is no significant difference ($P > 0.05$, t-test). (U) Comparison of percentage of neurons responding to tones (red), or to noise (blue) among different layers. N = 10, 5, 5, and 5 mice; 310, 104, 97, 95 cells, respectively. Bar = SD. L2/3 is significantly different from other layers. **$P < 0.01$, one-way ANOVA and post hoc test. (V) Percentage of responding cells in L2/3 in different frequency bands of A1. N = 87, 132, 91 cells.

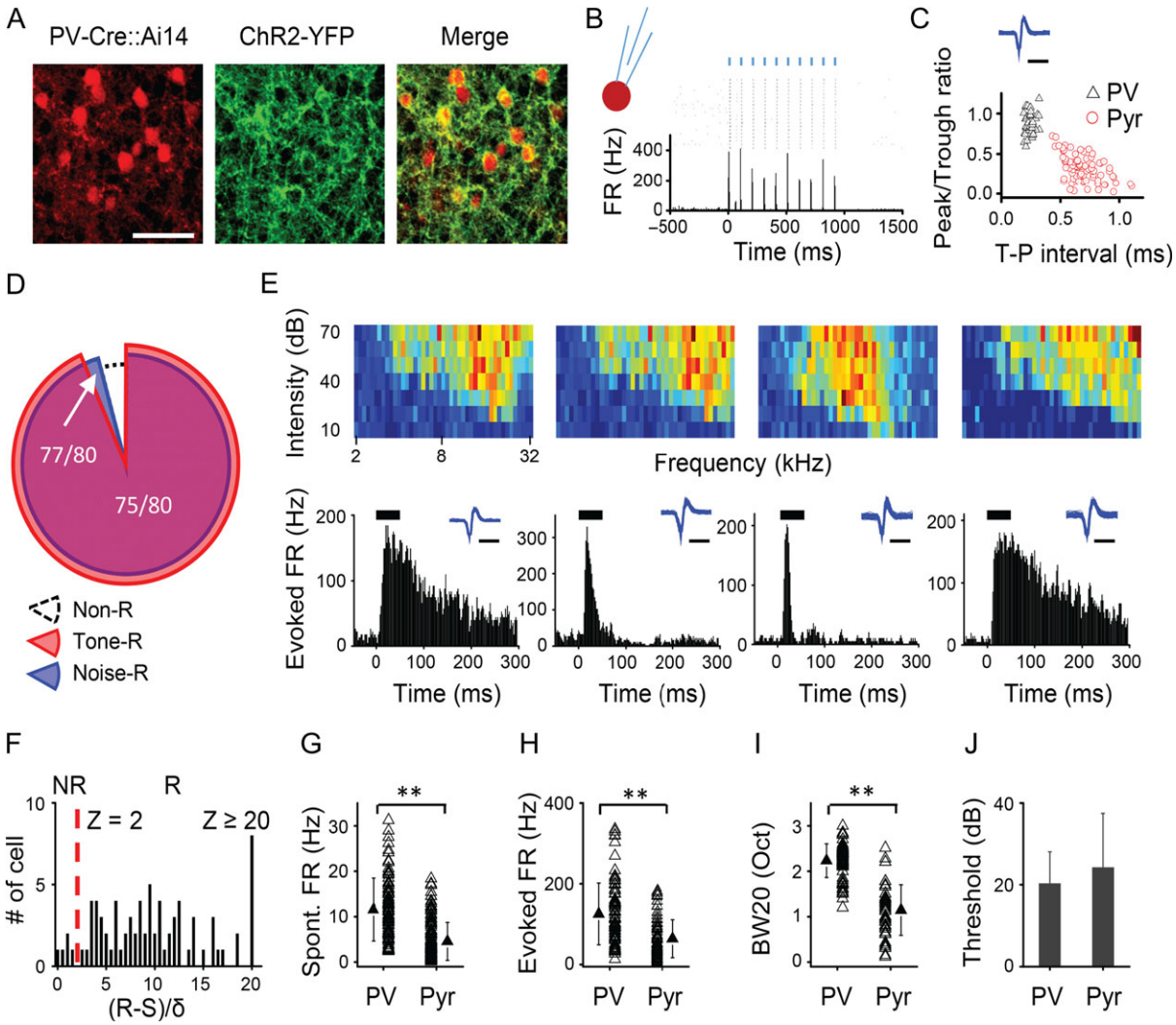

Figure 2. Sparse representation is absent in PV inhibitory neurons. (*A*) Confocal images show tdTomato-labeled PV neurons (red) and the expression of ChR2-YFP (green) in a representative slice. Scale bar, 200 μm. (*B*) Raster plot and PSTH for spike responses of a representative PV neuron to 10 pulses of blue LED stimulation (marked by blue vertical lines). (*C*) Plot of peak/trough amplitude ratio versus trough-to-peak interval for the spike waveforms of recorded PV and putative excitatory neurons. Each data point represents one cell. Inset, spike waveform for the PV cell shown in (*B*). Scale: 1 ms. (*D*) Proportion of PV cells responding to tones (red), or to noise (blue). (*E*) Color maps of TRF (top) and PSTHs (bottom) for best-tone-evoked spikes of 4 example PV cells. Inset, spike waveform of the corresponding cell. Scale: 1 ms. (*F*) Distribution of z-scores for identified PV cells (n = 80). (*G*) Comparison of spontaneous firing rate between L2/3 PV and pyramidal cells. $^{**}P < 0.01$, t-test. (*H*) Comparison of evoked firing rate. $^{**}P < 0.01$, t-test. (*I*) Comparison of TRF bandwidth (at 20 dB above the intensity threshold). $^{**}P < 0.01$, t-test. (*J*) Comparison of intensity threshold. $P = 0.1$, t-test.

In our voltage clamp recording, reasonably good clamping quality was demonstrated by a linear current–voltage (I–V) relationship for the recorded synaptic currents, as well as the closeness of the reversal potential of currents within a small time window immediately after the response onset observed at −70 mV (presumably pure excitatory currents) to the expected excitatory reversal potential (i.e., 0 mV) (Fig. 3*K*). In addition, from the experimentally observed excitation and inhibition, we derived the expected PSP response by integrating excitation and inhibition in a conductance-based single-compartment neuron model (Fig. 3*L–M*, see Materials and Methods). The amplitudes of derived PSP responses relatively well-separated NR and R neurons (Fig. 3*N*), suggesting that the observed synaptic inputs could largely account for the differential levels of recorded PSP responses (Fig. 3*C*). More importantly, for the majority of neurons the PSP response was below the observed spike threshold (Fig. 3*N*). In addition, the synaptic reversal potential calculated based on the momentary E/I ratio at the peak of PSP was in most of neurons more hyperpolarized than the spike threshold (Supplementary Fig. S4*I*). These findings are reminiscent of the previous study in the barrel cortex in which the synaptic reversal potential was directly measured (Crochet et al. 2011) and have well explained why the majority of neurons are NR cells. Altogether, our data indicate that E/I balance, including both factors of E/I ratio and absolute excitatory synaptic strength, plays a critical role in determining the differential responsiveness within the L2/3 excitatory neuron population.

Experience-dependent Developmental Emergence of Cortical Sparseness

Is sparse representation an intrinsic property of cortical circuits or does it arise during development? Next, we examined the

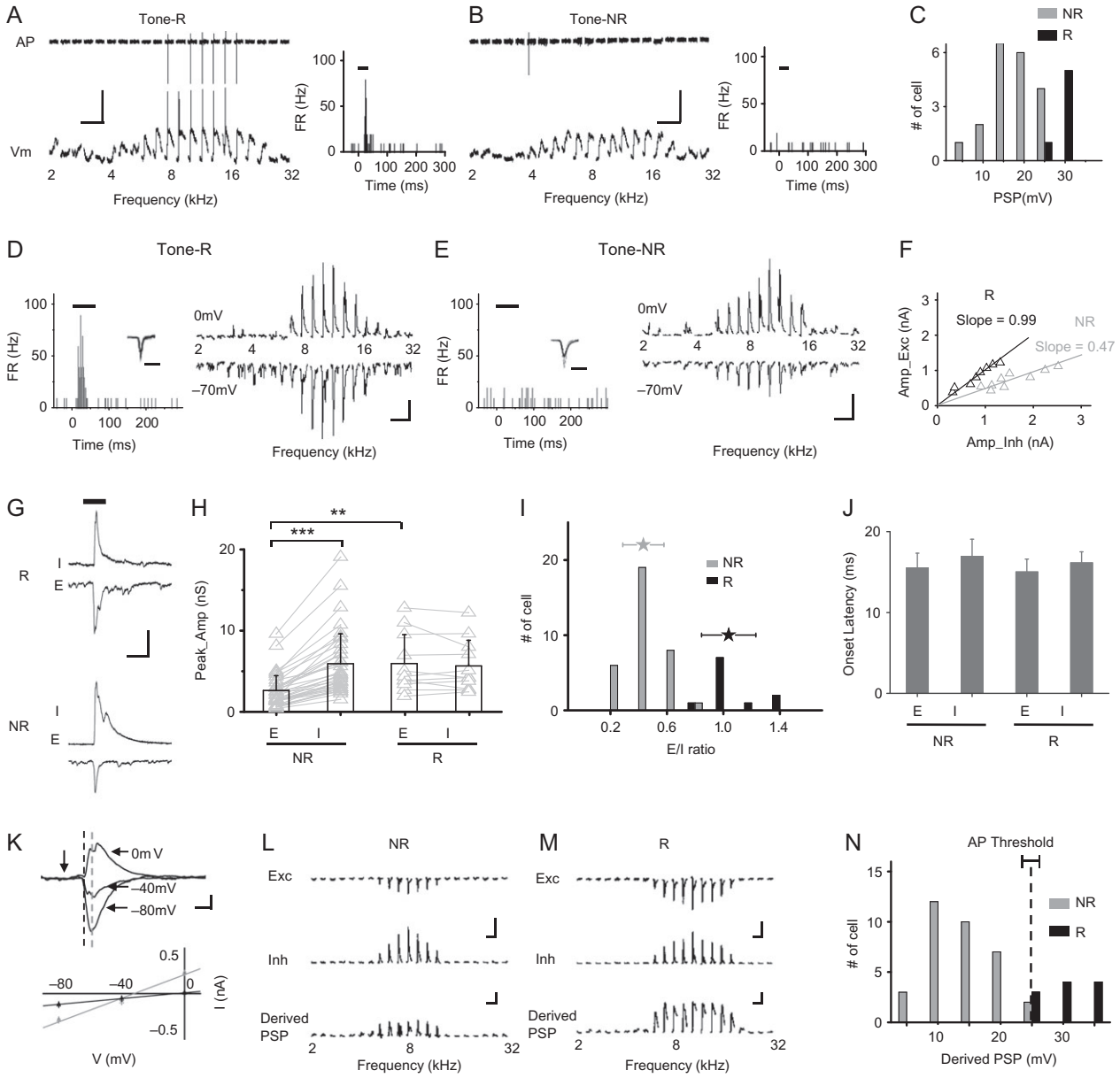

Figure 3. Synaptic mechanisms for the differential responsiveness of L2/3 excitatory neurons. (*A*) Left top, spike (AP) signals of an example R cell recorded in cell-attached mode in response to tones of different frequencies (only responses at 60 dB SPL intensity level are shown). Left bottom, membrane potential (V_m) responses of the same cell recorded in whole-cell current clamp mode. Scale: 30 mV, 100 ms. Right, PSTH for the evoked spikes. (*B*) An example NR cell displayed in a similar manner. (*C*) Distribution of peak amplitudes of PSP response evoked by the best tone. (*D*) Left, PSTH for spikes evoked by tones for a representative R cell. Tone duration is marked by the thick line. Inset, superimposed 100 spikes of the cell. Scale: 1 ms. Right, average excitatory (recorded at −70 mV, bottom) and inhibitory (at 0 mV, top) responses to tones of different frequencies (at 60 dB SPL). Scale: 500 pA, 100 ms. (*E*) A representative NR cell displayed in a similar manner as in (*D*). (*F*) Peak amplitude of excitation versus that of inhibition. The best-fit linear regression line is shown with its slope indicated. Black, for the R cell in (*D*); gray, for the NR cell in (*E*). (*G*) Enlargement of inhibitory (*I*) and excitatory (*E*) responses evoked by the best tone for the representative R (top) and NR (bottom) cell respectively. Scale: 1000 pA, 100 ms. (*H*) Comparison of peak amplitudes of excitation and inhibition between NR and R cells. Bar = SD. Individual cells are represented by gray symbols. Data points for the same cell are connected with a gray line. $N = 34$, and 11 cells for the NR and R group, respectively. $^{**}P < 0.01$; $^{***}P < 0.001$, Wilcoxon signed-rank test. (*I*) Distribution of E/I ratios for NR and R groups. Stars represent mean ± SD. (*J*) Average onset latencies (± SD) of excitation and inhibition evoked by the best tone. (*K*) Top, average synaptic currents of an example cell evoked by the best tone, recorded under different clamping voltages. Note that baseline currents have been subtracted. Scale: 100 pA, 25 ms. Vertical arrow marks the tone onset. Bottom, I–V relationship. The current value was an average within 1-ms window at 18-ms post-tone onset (marked by the dark dash line on top) and 28-ms post-tone onset (marked by the gray dash line), respectively. Bar = SE. Note that the reversal potential for the dark gray line is about 0 mV. (*L*) Experimentally observed excitation and inhibition, as well as derived PSP by integrating the excitation and inhibition for a NR cell. Scale: 500 pA (upper); 10 mV (lower), 300 ms. (*M*) Derived PSP responses for an R cell. Scale: 300 pA (upper); 10 mV (lower), 300 ms. (*N*) Distribution of derived PSPs to the best tone for the NR and R groups. The dash line marks the mean spike threshold (±SD) observed experimentally.

sparseness level in L2/3 of awake mice at different developmental stages (ST1, P18–P21; ST2, P25–P28; ST3, P32–P35). Surprisingly, at ST1, a majority of excitatory neurons responded to the noise/tone stimuli (Fig. 4A). The percentage of R cells was then progressively reduced during development (Fig. 4A). Along with the increase in the sparseness level, we also observed a drastic change in TRF properties (Fig. 4B). Specifically, the broadness of TRF, as measured by the bandwidth at 20 dB above the intensity

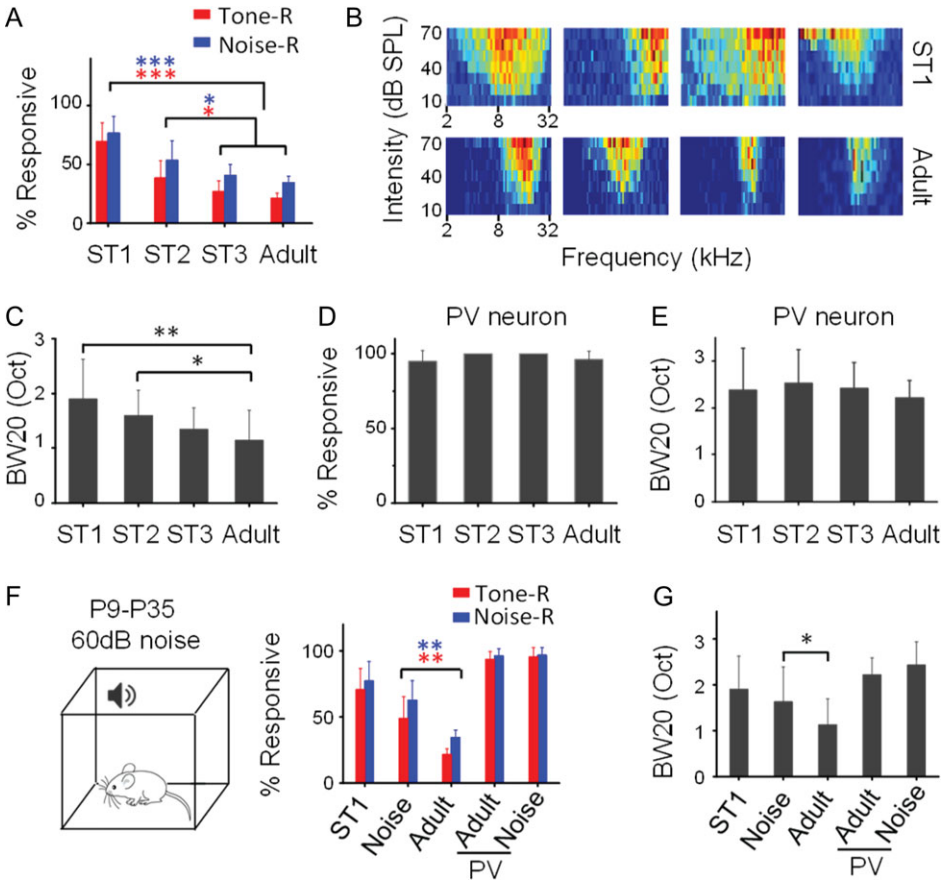

Figure 4. Experience-dependent developmental emergence of sparse representation in L2/3. (*A*) Percentage of L2/3 excitatory neurons responding to tones or to noise at different developmental stages. ST1, P18–P21; ST2, P25–P28; ST3: P32–P35. $N = 5, 5, 5$, and 10 mice; 130, 141, 119, and 310 cells, respectively. ***$P < 0.001$; *$P < 0.05$, one-way ANOVA and post hoc test. (*B*) Color maps of TRFs for 4 representative ST1 and adult neurons. (*C*) Comparison of TRF bandwidth at different stages. $N = 44$, 22, 15, and 45 cells, respectively. **$P < 0.01$; *$P < 0.05$, one-way ANOVA and post hoc test. (*D*) Percentage of PV inhibitory neurons responding to tones at different stages. $P > 0.5$, one-way ANOVA test. (*E*) TRF bandwidth of PV inhibitory neurons at different stages. $N = 17$, 12, 13, and 75 cells, respectively. $P > 0.5$, one-way ANOVA test. (*F*) Left, rearing the animal in a sound-attenuation chamber where noise was applied from P9 to P35. Right, percentage of responding L2/3 excitatory or PV neurons in ST1, noise-reared adult and control adult mice. Bar = SD. Noise-reared animals ($n = 5$ mice, 107 cells) are different from control adult animals for excitatory neurons (**$P < 0.01$, *t*-test). (*G*) Comparison of TRF bandwidth. $N = 23$ for excitatory cells and 23 for PV cells in the noise-reared group. *$P < 0.05$, *t*-test.

threshold (BW20), gradually reduced (Fig. 4*C*), consistent with previous reports that frequency selectivity of A1 neurons is sharpened during development (Zhang et al. 2001; Sun et al. 2010; Schreiner and Polley 2014). Therefore, our data demonstrate that cortical sparseness emerges developmentally along with the functional refinement of A1 neurons. In contrast to excitatory neurons, L2/3 PV inhibitory neurons remained highly responsive across developmental stages tested (Fig. 4*D*). Nor did the bandwidth of their TRFs reduce significantly during development (Fig. 4*E*). We did not observe significant changes of spontaneous FR across developmental stages in either the excitatory or PV cell population (Supplementary Fig. S5*A*,*B*).

We further investigated if the developmental emergence of cortical sparseness in L2/3 excitatory neurons could be influenced by early acoustic experience. We reared young animals in a noisy environment where continuous white noise was present for 12 h per day from P9 to P35 (see Materials and Methods), covering previously reported critical periods for auditory cortical plasticity (Zhang et al. 2002; Chang and Merzenich 2003; de Villers-Sidani et al. 2007; Barkat et al. 2011; Kim et al. 2013; Polley et al. 2013). Loose-patch recordings were performed in these mice at P45–P50. We found that noise rearing markedly impaired the developmental emergence of sparseness (Fig. 4*F*), as well as the developmental sharpening of TRFs of excitatory neurons (Fig. 4*G*), consistent with previous reports that noise exposure retards the functional development of A1 (Zhang et al. 2002; Chang and Merzenich 2003). Other TRF properties such as the intensity threshold and response latency were not significantly affected by noise rearing (Supplementary Fig. S5*C*, *D*). In contrast to excitatory neurons, in the PV cell population, neither the sparseness level nor the average TRF bandwidth was affected by noise rearing (Fig. 4*F*,*G*). Together, our data indicate that the developmental emergence of cortical sparseness as well as the functional refinement of L2/3 excitatory neurons is dependent on acoustic experience.

Changes of E/I Balance During Development

We further carried out sequential cell-attached and whole-cell recordings from L2/3 neurons in the immature A1 to examine if the developmental emergence of sparseness could be attributed to any changes in synaptic input. Overall, from ST1 to adult, there were moderate and unbalanced increases in the strength of excitation (Fig. 5*A*) and inhibition (Fig. 5*B*), which resulted in a significant decrease in E/I ratio (Fig. 5*C*). Different from the bimodal distribution of E/I ratios in adult, the distribution was unimodal

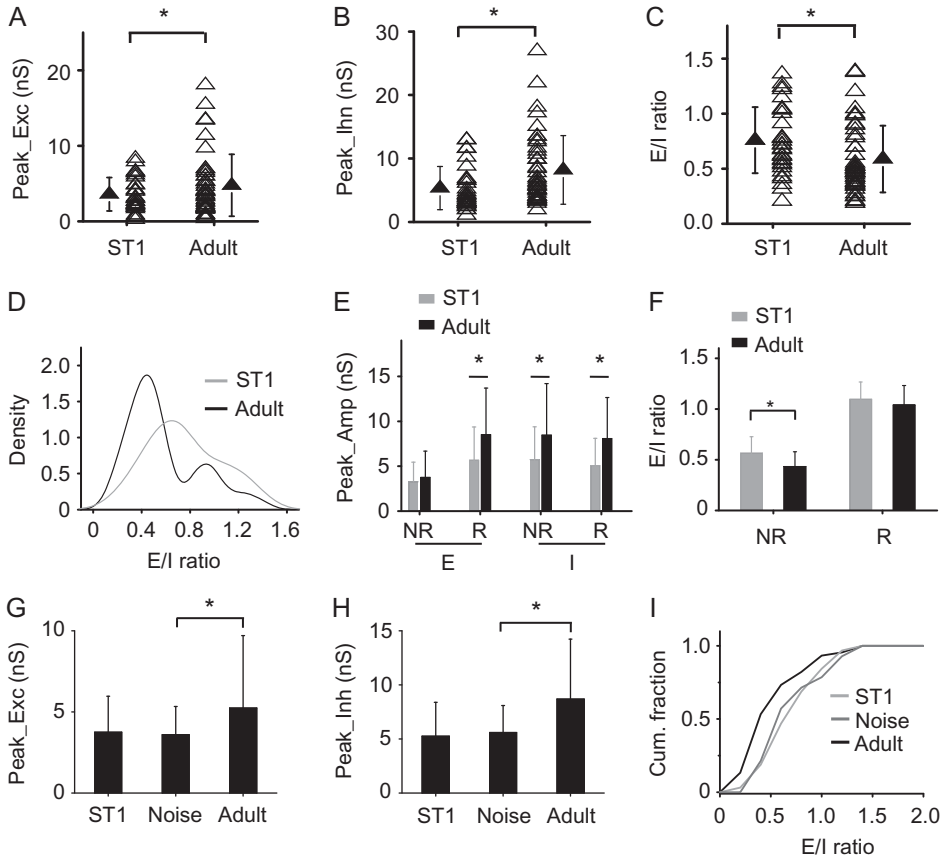

Figure 5. Synaptic mechanisms for the developmental enhancement of cortical sparseness. (*A*) Comparison of peak amplitude of excitation between ST1 and adult ages. *N* = 31 and 45 cells, respectively. Solid symbol represents mean ± SD. *P < 0.05, *t*-test. (*B*) Comparison of peak amplitude of inhibition. *P < 0.05, t-test. (*C*) Comparison of E/I ratio. *P < 0.05, *t*-test. (*D*) Distribution density of E/I ratios at ST1 and adult ages. The adult distribution is statistically bimodal, while the ST1 distribution is single-modal (see Statistical Test in Materials and Methods for details). (*E*) Average peak amplitudes of excitation and inhibition evoked by the best tone in the NR and R groups at ST1 and adult ages. *N* = 19 and 12 cells for R and NR group, respectively, at ST1. *P < 0.05, *t*-test. (*F*) Average E/I ratios in the NR and R groups. *P < 0.05, t-test. (*G*) Average peak amplitudes of excitation evoked by the best tone. *N* = 14 cells for the noise group. *P < 0.05, t-test. (*H*) Average peak amplitude of inhibition. *P < 0.05, *t*-test. (*I*) Cumulative fraction of E/I ratio for normal ST1 (light gray), noise-reared adult (dark gray) and normally reared adult (dark) animals. There is a significant difference between noise and control adult groups (*P* < 0.05, KS test).

at ST1 (Fig. 5*D*), indicating that during development a substantial fraction of neurons lowered their E/I ratios. We next examined R and NR groups separately. For the R group, there were significant increases of both excitation and inhibition during development, whereas for the NR group significant increase was only observed for inhibition but not excitation (Fig. 5*E*). Considering that there is an increase in the number of NR cells during development (Fig. 4A), the latter result implies that for some NR neurons converted from R cells, the excitation they received was in fact weakened, despite the overall strengthening of excitation for the entire population. Therefore, the excitatory input strength is differentially modulated within the excitatory cell population. Along with a general, unselective strengthening of inhibition (Fig. 5*E*), the average E/I ratio in the NR group was reduced, while it was not significantly changed in the R group (Fig. 5*F*). We further derived PSP responses from the observed excitation and inhibition at ST1, using the same membrane parameters as for adult cells. The derived PSP responses were significantly stronger than in adult (Supplementary Fig. S6), consistent with the observation that there was a higher fraction of R neurons during early development. These results indicate that the change in E/I balance alone can explain the developmental enhancement of sparseness, although some other factors, for example, changes in membrane properties, may also contribute.

Finally, we examined excitatory and inhibitory inputs in animals which had been exposed to noise during development. We found that noise rearing prevented the overall developmental increase in the strength of excitation (Fig. 5*G*) and inhibition (Fig. 5*H*), as well as the developmental change in the distribution of E/I ratios (Fig. 5*I*). Thus, disrupting the normal acoustic environment during early development impairs the developmental maturation of E/I balance, contributing to the disruption of emergence of cortical sparseness.

Modulating Sparseness Level by Manipulating PV or L1 Inhibitory Neuron Activity

Our data have suggested a key role of E/I balance in determining sparseness level in the cortex. We wondered whether sparseness level could be changed acutely by manipulating E/I balance. PV neurons are known to contribute importantly to the E/I balance of sensory-evoked responses in the cortex (Atallah et al. 2012; Li et al. 2014). To manipulate PV neuron activity, we injected AAV encoding Cre-dependent ArchT into A1 of adult PV-Cre mice and delivered green LED light to suppress ArchT-expressing PV neurons (Fig. 6A). TRF mapping for an example cell is shown in Fig. 6*B*. The cell was originally an NR cell, as no TRF could be identified (Fig. 6*B*, left panel). When tone stimuli

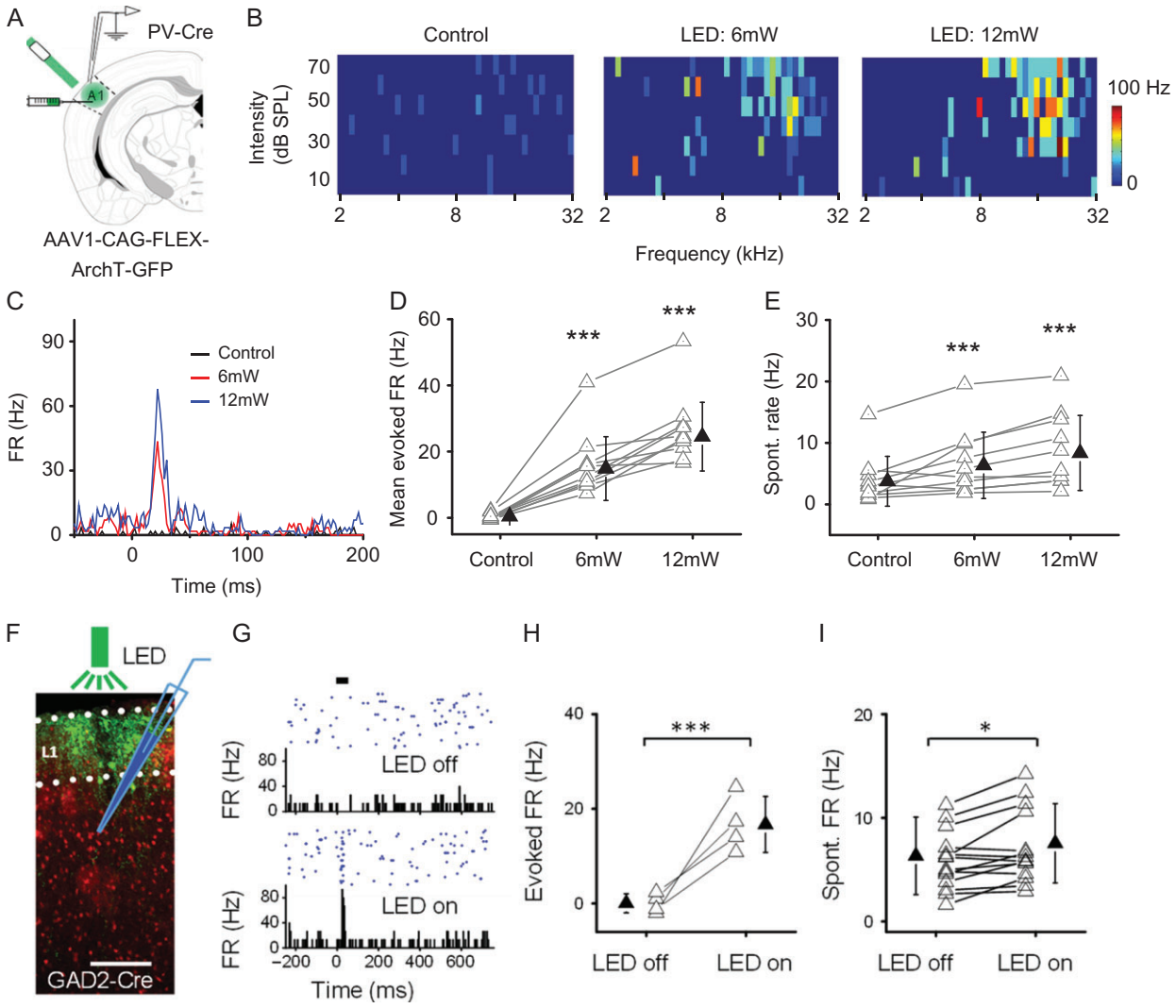

Figure 6. Manipulations of the sparse level by 2 methods. **I.** Suppressing PV inhibitory neurons reduces sparseness level. (*A*) Injection of AAV encoding Cre-dependent ArchT into A1 of PV-Cre mice. Green LED light was applied to A1 surface. Loose-patch recording was made in A1. (*B*) Mapped TRFs in a putative L2/3 excitatory neuron in the control condition (left) and when tone stimuli were coupled with LED stimulation at 6 mW (middle) and 12 mW (right) power. (*C*) PSTH for spike responses to all test tones for the same cell shown in (*B*). (*D*) Average firing rate evoked by the best tone as observed in the condition of 6- and 12-mW LED stimulation. $N = 10$ cells. ***$P < 0.001$, one-way ANOVA and post hoc test (compared with control). (*E*) Spontaneous firing rate measured within 50-ms window preceding tone onset in control and LED stimulation conditions. ***$P < 0.001$, one-way ANOVA and post hoc test (compared with control). **II.** Suppressing L1 inhibitory neurons reduces sparseness level. (*F*) Expression of ArchT (green) in GAD2-Cre::Ai14 mice. Green LED was applied to A1 surface. Loose-patch recording was made from L2/3. (*G*) Responses of a putative L2/3 excitatory neuron to noise stimulation (thick bar) in the control condition (top) and when noise was coupled with LED illumination (bottom). (*H*) Noise-evoked firing rates of 4 L2/3 neurons converted from NR to R cells. ***$P < 0.001$, *t*-test. (*I*) Spontaneous firing rates of 15 L2/3 neurons examined in the control and LED on conditions. *$P < 0.05$, *t*-test.

were coupled with LED illumination, spike responses and a V-shaped TRF appeared (Fig. 6*B*, middle panel, and Fig. 6*C*), which resembled those of a de novo R cell. The TRF appeared more distinctive and tone-evoked FR was higher when higher LED power was applied (Fig. 6*B*, right panel, and Fig. 6*C*). Similar phenomena were observed in 10 cells originally identified as NR cells (Fig. 6*D*). The spontaneous FR of these cells was also increased by LED illumination alone (Fig. 6*E*), consistent with the notion of reduced inhibition. Our data thus demonstrate that NR cells can be converted to R cells, that is, sparseness level can be reduced, by suppressing PV inhibitory neurons.

Previous studies have suggested that cortical layer 1, containing only inhibitory neurons, can play a role in modulating sensory-evoked responses in L2/3 (Letzkus et al. 2011; Zhou et al. 2014; Ibrahim et al. 2016; Takesian et al. 2018). We thus wondered whether manipulating L1 neuron activity could also affect sparseness level in L2/3. We expressed ArchT in L1 neurons by local iontophoretic injections of AAV vectors in GAD2-Cre mice (Fig. 6*F*), following our previous study (Ibrahim et al. 2016). As shown by an example L2/3 neuron (Fig. 6*G*), the cell initially did not respond to noise with increased spiking, but a transient spike rate increase appeared when noise was paired with green LED light. In 4 out of the 15 tested L2/3 excitatory neurons, we observed a similar appearance of noise-evoked response when L1 neurons were optogenetically suppressed (Fig. 6*H*). Spontaneous firing rates of these tested neurons were

also increased (Fig. 6*I*), supporting a general inhibitory effect of L1 activation on L2/3 pyramidal cells (Jiang et al. 2013). Thus, our data suggest that activation of L1, either by long-range top-down or bottom-up inputs (Letzkus et al. 2011; Cruz-Martin et al. 2014; Ibrahim et al. 2016; Ji et al. 2016; Takesian et al. 2018), can enhance the sparseness level in L2/3.

Discussion

Sparse Representation in the Auditory Cortex

In the auditory cortex, previously several studies have reported response sparseness, that is, only a small fraction of neurons respond with spike rate increases to a given type of sound (Sutter et al. 1999; Hromadka et al. 2008; Chambers et al. 2014; Issa et al. 2014; Kato et al. 2015). In awake marmosets, it is suggested that as long as a proper auditory stimulus is found almost every A1 neuron can be driven vigorously (Wang et al. 2005). However, it is probably impractical to test every possible stimulus. In this study, by cross-examining neuronal responsiveness, we found a large overlap between responsiveness of simple sounds, such as tones and noise, and many other more complex sounds. In particular, a noise-responsive neuron can respond to almost all the sound types tested. Out of hundreds of neurons recorded, we only found a few cells that, while responding to tones, were not driven by broadband noise. In other words, when the type of sound is considered, selectivity of the responding neurons appear somewhat weak, while within a specific sound category a neuron's selectivity can be well characterized (e.g., as the preferred tone frequency or preferred direction of FM sweeps). For the majority of neurons that remained nonresponding under any tested sound categories, it is still possible that they are selective for some special auditory features not included in our stimulus sets. In other words, these neurons may exhibit extremely high selectivity or lifetime sparseness (Vinje and Gallant 2000; Willmore and Tolhurst 2001). In the future, the preferred stimulus of these neurons may be identified by using stimulus evolution techniques that allow rapid tailoring of stimulus features according to real-time variations in neuronal firing rate (Chambers et al. 2014).

Due to their large coverage of other sound types in terms of responsiveness, noise and tones could be used to evaluate a lower bound of cortical sparseness and to explore the mechanisms underlying differential responsiveness within the neuronal population. We found that noise can drive about one-third of L2/3 excitatory neurons in A1, supporting the previous observations of sparse representation in the primary auditory cortex (Issa et al. 2014; Kato et al. 2015). Sparseness level is not only dependent on stimulus type but may also depend on the cortical area examined. For example, the mouse visual cortex appears to have a lower sparseness level than auditory and somatosensory cortices, as Ca^{2+} imaging studies have shown that about 50–60% of visual cortical neurons in superficial layers respond to a natural scene movie (Kampa et al. 2011; Ko et al. 2011). In addition, sparseness level may be influenced by the brain or behavioral state, since the internal state of the brain also plays a role in modulating neuronal responses (Crochet and Petersen 2006; McGinley et al. 2015). Recently, it has been reported that locomotion reduces auditory cortical responses relative to the stationary state (Schneider et al. 2014; Zhou et al. 2014). Since our recordings were carried out mostly in the stationary state, it is expected that in the locomotion state the sparseness level could be even higher than observed in this study.

Laminar and Cell-type Dependence

We demonstrate that sparseness level is dependent on laminar location. It is much higher in L2/3 than the other layers, suggesting that local L2/3 circuits contribute primarily to the enhancement of sparseness. It has been suggested that this cortical layer performs more elaborate sensory processing, as manifested by more pronounced tuning for some sensory features (Adesnik et al. 2012; Petersen and Crochet 2013; Li et al. 2014). Sparse representation could then be an outcome of the specialization of sensory processing functions. Sparse representation is absent in the L2/3 PV inhibitory neuron population, as nearly all the PV cells respond to noise and tones. This property is consistent with a generally weak selectivity in sensory responses of these cells (Kerlin et al. 2010; Ma et al. 2010; Hofer et al. 2011; Kuhlman et al. 2011; Li et al. 2015; Scholl et al. 2015). The high-level responsiveness of PV neurons as well as their weak selectivity can be explained by the broad connectivity of this cell type with nearly all nearby excitatory neurons (Fino and Yuste 2011).

In a recent study, it has been reported that L3 excitatory neurons have lower responsiveness than L2 excitatory neurons, and that they are morphologically distinct (Oviedo et al. 2010). In the current study, R and NR cells did not appear to differ in dendritic morphology or cortical depth (Supplementary Fig. S3*F–H*). Therefore, it is unlikely that the R and NR cells specifically correspond to L2 and L3 neurons described in the previous study. More likely, the R and NR cells belong to the same pyramidal cell class receiving different levels of synaptic input.

Synaptic Mechanisms Underlying Sparse Representation

Using sequential cell-attached and whole-cell recordings, we have been able to directly investigate the excitatory and inhibitory synaptic mechanisms underlying the sparse representation. First of all, it cannot be attributed to sparse synaptic input. Regardless of R or NR cells, the recorded neurons always exhibited auditory-evoked excitatory and inhibitory inputs, suggesting that all neurons in the circuit can be engaged by auditory stimulation. Second, we found that R and NR neurons differ in the strength of excitatory but not inhibitory input. They do not differ in other properties such as resting membrane potential, input resistance or spike threshold. The strong correlation between responsiveness and excitatory input strength observed in this study raises a concern of whether the weaker excitation observed in some cells could be due to damages of apical dendrites and excitatory synapses on these dendrites by the recording electrodes, whereas inhibition could be much less affected since inhibitory synapses might be mostly peri-somatic. However, our results from noise-rearing experiments argue against this possibility: the manipulation of sensory environment during development changes the sparseness level and E/I ratio in the adult cortex, but there is no reason to assume that such manipulation would affect the chances of damaging apical dendrites in the recording procedure. Together, our results suggest that the differential levels of excitatory drive (i.e., synaptic amplitude) and E/I ratio contribute primarily to the differential responsiveness within the excitatory cell population, considering that E/I ratio determines the reversal potential of synaptic response (Borg-Graham et al. 1998) and excitatory drive largely determines whether the membrane potential response can possibly reach the expected

reversal potential. The relatively more homogenous inhibitory input strength is consistent with the high responsiveness of PV inhibitory neurons, which ensures that excitatory neurons receive a blanket of inhibition (Fino and Yuste 2011) under any given sensory stimuli. This finding is consistent with a proposed role of inhibition in regulating sparse responses (Poo and Isaacson 2009; Crochet et al. 2011).

By using 2 methods (optogenetically suppressing PV or L1 inhibitory neurons) to manipulate E/I balance in L2/3 neurons, we found that it was possible to acutely turn NR into R cells and thus reduce sparseness level. These results support the critical role of E/I balance in determining responsiveness. Interestingly, a recent study suggests that cortical circuits can compensate for reduced inhibition so that optogenetically suppressing PV neurons results in unexpected increases of both excitation and inhibition to L2/3 pyramidal neurons (Moore et al. 2018). If this is the case, then the enhancement of evoked firing in L2/3 pyramidal neurons under optogenetic suppression of PV cells may be attributed mainly to the increased excitation, but not necessarily decreased inhibition. As for the L1 manipulation, it has been suggested that L1 interneurons can mediate both the centered disinhibitory and surrounding inhibitory circuits (Jiang et al. 2013; Larkum 2013; Lee et al. 2015). Therefore, suppressing L1 neurons unselectively may produce a mixture of both inhibitory and disinhibitory effects. It is possible that by selectively suppressing surround or center L1 neurons, sparseness level could be manipulated in opposite directions. Such modulation of sparseness level could be potentially achieved via long-range projections into L1 (Letzkus et al. 2011; Ibrahim et al. 2016). Together, our finding of E/I balance playing a critical role in determining sparse representation is consistent with its reported impacts on neuronal output responses (Poo and Isaacson 2009; Liu et al. 2011; Wu et al. 2011; Atallah et al. 2012; Li et al. 2014; Yu et al. 2014).

Developmental Emergence of Sparse Representation

Previously, sparse representation has not been examined in developing sensory cortices. In the current study, the establishment of stable unbiased recordings in awake immature A1 allowed us to address this issue. We have now demonstrated that sparse representation in L2/3 emerges during postnatal development. This process is accompanied by a progressive sharpening of neuronal TRFs. By the end of a critical period for the cortical development of frequency representation (Kim et al. 2013), the sparseness has reached a similar level as in adult. The emergence of sparse representation is experience-dependent. Disruption of a normal acoustic environment with noise exposure impaired the developmental emergence of sparse representation, as well as the developmental sharpening of neuronal TRFs. These results suggest that sparse representation may result from the functional differentiation of A1 neurons (Zhang et al. 2001; Sun et al. 2010). Similar as receptive field properties, sparse representation can be an indicator for the functional maturation of cortical circuits.

Similar as in adult, R cells in the developing A1 generally have higher E/I ratios than NR cells. However, the distribution of E/I ratios in the entire population is different between young and adult ages. In early development, it is consistent with a normal distribution, suggesting that the initial formation of synaptic connections is through stochastic processes. With development, the proportion of neurons with lower E/I ratios is significantly increased, resulting in an overall decrease in E/I ratio and changing from a unimodal to bimodal distribution of E/I ratios. In other words, there is more separation between NR and R cells. Since E/I balance determines the synaptic reversal potential, the lower E/I ratio (i.e., more hyperpolarized synaptic reversal potential) in the NR group (Fig. 5F) implies that it is even harder for this group of cells to spike. This lowering of E/I ratio in the NR group can be attributed to selective weakening of excitation in some cells and unselective strengthening of inhibition in all cells. Together, the developmental changes in E/I balance would result in reduced responsiveness, and possibly combining with other changes, for example, those in membrane properties, lead to the emergence of sparse representation.

As our data from noise-reared animals have supported a critical role of experience in the developmental emergence of response sparseness, it is possible that sensory related activity, when kicks in, shapes the network connectivity by selectively stabilizing/strengthening some connections while weakening many others (Ko et al. 2011; Xue et al. 2014; Cossell et al. 2015). A previous slice recording study on L2/3 pyramidal neurons in the mouse visual cortex suggests that through developmental plasticity inhibition can be matched to the different amounts of excitation in individual pyramidal cells so that E/I ratios are equalized across the pyramidal cell population (Xue et al. 2014). In the present study, our data on sound-evoked responses in auditory cortex in vivo, however, suggest that E/I ratio is regulated specifically in individual pyramidal cells and can be different between different subsets of these neurons. While this may reflect a difference between different sensory modalities, our results suggest that differentially regulating E/I balance in individual cells may be important for optimizing sensory representation of the external world.

Implications for Nonresponding Neurons

That the majority of excitatory neurons in L2/3 of A1 are not driven by any of our testing sound stimuli is surprising. Here, we propose the following scenarios for the potential functional relevance of these “silent” neurons. First, they may be functionally very specialized, that is, they only respond to some specialized sound features (e.g., features of vocalization sounds) which are not included in our test sets. Second, although auditory input alone is not sufficient to drive these neurons, combining with some other inputs (e.g., neuromodulatory or cross-modal sensory inputs) may be able to drive them. Third, as these neurons all receive auditory-evoked synaptic inputs, they have the potential to boost their responsiveness through changing synaptic strengths, which could occur during learning processes (Weinberger and Bakin 1998; Letzkus et al. 2011; Nabavi et al. 2014). In other words, these neurons may serve as a large reserve pool of undercommitted sensory neurons to be recruited under specific conditions as the cortex adapts to the changing external environment. It is of particular interest to investigate in the future under what natural conditions new responses to any features of auditory stimuli can be induced in the NR neurons, as a recent study in hippocampal CA1 neurons has shown that appropriately timed, conjunctive CA3 and entorhinal cortical inputs can induce the formation of new place fields in initially silent cells (Bittner et al. 2015). Finally, even without spiking responses, the NR neurons may still be able to influence sensory coding, since their subthreshold responses can contribute to the local field potential and may affect synchronous firing of other neurons and thus oscillatory activity in the local circuit (Barth and Poulet 2012). Future investigations will be needed to test these intriguing possibilities.

Supplementary Material

Supplementary material is available at *Cerebral Cortex* online.

Funding

The US National Institutes of Health (grant R01DC008983 to L.I.Z.). The US National Institutes of Health (grant R01EY019049 to H.W.T.). The National Natural Science Foundation of China (31671084 to F.L.).

Notes

L.I.Z. and H.W.T. conceived the study. F.L. and H.L. performed most of the in vivo experiments. F.L. performed most data analysis. X.C., M.Z., and N.K.Z contributed to data collection and analysis. K.K.Z. performed statistical tests on bimodality. Z.X. helped with the discussion. H.W.T. and L.I.Z. wrote the manuscript. *Conflict of Interest*: None declared.

References

Adesnik H, Bruns W, Taniguchi H, Huang ZJ, Scanziani M. 2012. A neural circuit for spatial summation in visual cortex. Nature. 490(7419):226–231.

Atallah BV, Bruns W, Carandini M, Scanziani M. 2012. Parvalbumin-expressing interneurons linearly transform cortical responses to visual stimuli. Neuron. 73(1):159–170.

Barkat TR, Polley DB, Hensch TK. 2011. A critical period for auditory thalamocortical connectivity. Nat Neurosci. 14(9): 1189–1194.

Barth AL, Poulet JF. 2012. Experimental evidence for sparse firing in the neocortex. Trends Neurosci. 35(6):345–355.

Bittner KC, Grienberger C, Vaidya SP, Milstein AD, Macklin JJ, Suh J, Tonegawa S, Magee JC. 2015. Conjunctive input processing drives feature selectivity in hippocampal CA1 neurons. Nat Neurosci. 18(8):1133–1142.

Borg-Graham LJ, Monier C, Fregnac Y. 1998. Visual input evokes transient and strong shunting inhibition in visual cortical neurons. Nature. 393(6683):369–373.

Chambers AR, Hancock KE, Sen K, Polley DB. 2014. Online stimulus optimization rapidly reveals multidimensional selectivity in auditory cortical neurons. J Neurosci. 34(27): 8963–8975.

Chang EF, Merzenich MM. 2003. Environmental noise retards auditory cortical development. Science. 300(5618):498–502.

Cossell L, Iacaruso MF, Muir DR, Houlton R, Sader EN, Ko H, Hofer SB, Mrsic-Flogel TD. 2015. Functional organization of excitatory synaptic strength in primary visual cortex. Nature. 518(7539):399–403.

Crochet S, Petersen CC. 2006. Correlating whisker behavior with membrane potential in barrel cortex of awake mice. Nat Neurosci. 9(5):608–610.

Crochet S, Poulet JF, Kremer Y, Petersen CC. 2011. Synaptic mechanisms underlying sparse coding of active touch. Neuron. 69(6):1160–1175.

Cruz-Martin A, El-Danaf RN, Osakada F, Sriram B, Dhande OS, Nguyen PL, Callaway EM, Ghosh A, Huberman AD. 2014. A dedicated circuit links direction-selective retinal ganglion cells to the primary visual cortex. Nature. 507 (7492):358–361.

de Villers-Sidani E, Chang EF, Bao S, Merzenich MM. 2007. Critical period window for spectral tuning defined in the primary auditory cortex (A1) in the rat. J Neurosci. 27(1): 180–189.

Epsztein J, Brecht M, Lee AK. 2011. Intracellular determinants of hippocampal CA1 place and silent cell activity in a novel environment. Neuron. 70(1):109–120.

Fenno L, Yizhar O, Deisseroth K. 2011. The development and application of optogenetics. Annu Rev Neurosci. 34:389–412.

Fino E, Yuste R. 2011. Dense inhibitory connectivity in neocortex. Neuron. 69(6):1188–1203.

Guo W, Chambers AR, Darrow KN, Hancock KE, Shinn-Cunningham BG, Polley DB. 2012. Robustness of cortical topography across fields, laminae, anesthetic states, and neurophysiological signal types. J Neurosci. 32(27): 9159–9172.

Hackett TA, Barkat TR, O'Brien BM, Hensch TK, Polley DB. 2011. Linking topography to tonotopy in the mouse auditory thalamocortical circuit. J Neurosci. 31(8):2983–2995.

Hahnloser RH, Kozhevnikov AA, Fee MS. 2002. An ultra-sparse code underlies the generation of neural sequences in a songbird. Nature. 419(6902):65–70.

Hofer SB, Ko H, Pichler B, Vogelstein J, Ros H, Zeng H, Lein E, Lesica NA, Mrsic-Flogel TD. 2011. Differential connectivity and response dynamics of excitatory and inhibitory neurons in visual cortex. Nat Neurosci. 14(8):1045–1052.

Hromadka T, Deweese MR, Zador AM. 2008. Sparse representation of sounds in the unanesthetized auditory cortex. PLoS Biol. 6(1):e16.

Ibrahim LA, Mesik L, Ji XY, Fang Q, Li HF, Li YT, Zingg B, Zhang LI, Tao HW. 2016. Cross-modality sharpening of visual cortical processing through layer-1-mediated inhibition and disinhibition. Neuron. 89(5):1031–1045.

Isaacson JS, Scanziani M. 2011. How inhibition shapes cortical activity. Neuron. 72(2):231–243.

Issa JB, Haeffele BD, Agarwal A, Bergles DE, Young ED, Yue DT. 2014. Multiscale optical Ca2+ imaging of tonal organization in mouse auditory cortex. Neuron. 83(4):944–959.

Ji XY, Zingg B, Mesik L, Xiao Z, Zhang LI, Tao HW. 2016. Thalamocortical innervation pattern in mouse auditory and visual cortex: laminar and cell-type specificity. Cereb Cortex. 26(6):2612–2625.

Jiang X, Wang G, Lee AJ, Stornetta RL, Zhu JJ. 2013. The organization of two new cortical interneuronal circuits. Nat Neurosci. 16(2):210–218.

Kampa BM, Roth MM, Gobel W, Helmchen F. 2011. Representation of visual scenes by local neuronal populations in layer 2/3 of mouse visual cortex. Front Neural Circuits. 5:18.

Kato HK, Gillet SN, Isaacson JS. 2015. Flexible sensory representations in auditory cortex driven by behavioral relevance. Neuron. 88(5):1027–1039.

Kerlin AM, Andermann ML, Berezovskii VK, Reid RC. 2010. Broadly tuned response properties of diverse inhibitory neuron subtypes in mouse visual cortex. Neuron. 67(5): 858–871.

Kim H, Gibboni R, Kirkhart C, Bao S. 2013. Impaired critical period plasticity in primary auditory cortex of fragile X model mice. J Neurosci. 33(40):15686–15692.

Ko H, Hofer SB, Pichler B, Buchanan KA, Sjostrom PJ, Mrsic-Flogel TD. 2011. Functional specificity of local synaptic connections in neocortical networks. Nature. 473(7345):87–91.

Kuhlman SJ, Tring E, Trachtenberg JT. 2011. Fast-spiking interneurons have an initial orientation bias that is lost with vision. Nat Neurosci. 14(9):1121–1123.

Larkum ME. 2013. The yin and yang of cortical layer 1. Nat Neurosci. 16(2):114–115.

Laughlin SB, Sejnowski TJ. 2003. Communication in neuronal networks. Science. 301(5641):1870–1874.

Lee AJ, Wang G, Jiang X, Johnson SM, Hoang ET, Lanté F, Stornetta RL, Beenhakker MP, Shen Y, Zhu JJ. 2015. Canonical organization of layer 1 neuron-led cortical inhibitory and disinhibitory interneuronal circuits. Cereb Cortex. 25(8):2114–2126.

Letzkus JJ, Wolff SB, Meyer EM, Tovote P, Courtin J, Herry C, Luthi A. 2011. A disinhibitory microcircuit for associative fear learning in the auditory cortex. Nature. 480(7377):331–335.

Levy WB, Baxter RA. 1996. Energy efficient neural codes. Neural Comput. 8(3):531–543.

Li LY, Ji XY, Liang F, Li YT, Xiao Z, Tao HW, Zhang LI. 2014. A feedforward inhibitory circuit mediates lateral refinement of sensory representation in upper layer 2/3 of mouse primary auditory cortex. J Neurosci. 34(41):13670–13683.

Li LY, Li YT, Zhou M, Tao HW, Zhang LI. 2013. Intracortical multiplication of thalamocortical signals in mouse auditory cortex. Nat Neurosci. 16(9):1179–1181.

Li LY, Xiong XR, Ibrahim LA, Yuan W, Tao HW, Zhang LI. 2015. Differential receptive field properties of parvalbumin and somatostatin inhibitory neurons in mouse auditory cortex. Cereb Cortex. 25(7):1782–1791.

Liu BH, Li YT, Ma WP, Pan CJ, Zhang LI, Tao HW. 2011. Broad inhibition sharpens orientation selectivity by expanding input dynamic range in mouse simple cells. Neuron. 71(3):542–554.

Liu BH, Li P, Sun YJ, Li YT, Zhang LI, Tao HW. 2010. Intervening inhibition underlies simple-cell receptive field structure in visual cortex. Nat Neurosci. 13(1):89–96.

Ma WP, Liu BH, Li YT, Huang ZJ, Zhang LI, Tao HW. 2010. Visual representations by cortical somatostatin inhibitory neurons—selective but with weak and delayed responses. J Neurosci. 30 (43):14371–14379.

McGinley MJ, David SV, McCormick DA. 2015. Cortical membrane potential signature of optimal states for sensory signal detection. Neuron. 87(1):179–192.

Moore AK, Weible AP, Balmer TS, Trussell LO, Wehr M. 2018. Rapid rebalancing of excitation and inhibition by cortical circuitry. Neuron. 97(6):1341–1355.

Nabavi S, Fox R, Proulx CD, Lin JY, Tsien RY, Malinow R. 2014. Engineering a memory with LTD and LTP. Nature. 511(7509): 348–352.

Olshausen BA, Field DJ. 2004. Sparse coding of sensory inputs. Curr Opin Neurobiol. 14(4):481–487.

Oviedo HV, Bureau I, Svoboda K, Zador AM. 2010. The functional asymmetry of auditory cortex is reflected in the organization of local cortical circuits. Nat Neurosci. 13(11): 1413–1420.

Perez-Orive J, Mazor O, Turner GC, Cassenaer S, Wilson RI, Laurent G. 2002. Oscillations and sparsening of odor representations in the mushroom body. Science. 297(5580):359–365.

Petersen CC, Crochet S. 2013. Synaptic computation and sensory processing in neocortical layer 2/3. Neuron. 78(1):28–48.

Polley DB, Thompson JH, Guo W. 2013. Brief hearing loss disrupts binaural integration during two early critical periods of auditory cortex development. Nat Commun. 4:2547.

Poo C, Isaacson JS. 2009. Odor representations in olfactory cortex: "sparse" coding, global inhibition, and oscillations. Neuron. 62(6):850–861.

Rudy B, Fishell G, Lee S, Hjerling-Leffler J. 2011. Three groups of interneurons account for nearly 100% of neocortical GABAergic neurons. Dev Neurobiol. 71(1):45–61.

Sakata S, Harris KD. 2009. Laminar structure of spontaneous and sensory-evoked population activity in auditory cortex. Neuron. 64(3):404–418.

Schneider DM, Nelson A, Mooney R. 2014. A synaptic and circuit basis for corollary discharge in the auditory cortex. Nature. 513(7517):189–194.

Scholl B, Pattadkal JJ, Dilly GA, Priebe NJ, Zemelman BV. 2015. Local integration accounts for weak selectivity of mouse neocortical parvalbumin interneurons. Neuron. 87(2):424–436.

Schreiner CE, Polley DB. 2014. Auditory map plasticity: diversity in causes and consequences. Curr Opin Neurobiol. 24(1): 143–156.

Shoham S, O'Connor DH, Segev R. 2006. How silent is the brain: is there a "dark matter" problem in neuroscience? J Comp Physiol A Neuroethol Sens Neural Behav Physiol. 192(8):777–784.

Sun YJ, Wu GK, Liu BH, Li P, Zhou M, Xiao Z, Tao HW, Zhang LI. 2010. Fine-tuning of pre-balanced excitation and inhibition during auditory cortical development. Nature. 465(7300):927–931.

Sutter ML, Schreiner CE, McLean M, O'Connor KN, Loftus WC. 1999. Organization of inhibitory frequency receptive fields in cat primary auditory cortex. J Neurophysiol. 82(5):2358–2371.

Takesian AE, Bogart LJ, Lichtman JW, Hensch TK. 2018. Inhibitory circuit gating of auditory critical-period plasticity. Nat Neurosci. 21(2):218–227.

Vinje WE, Gallant JL. 2000. Sparse coding and decorrelation in primary visual cortex during natural vision. Science. 287 (5456):1273–1276.

Wang X, Lu T, Snider RK, Liang L. 2005. Sustained firing in auditory cortex evoked by preferred stimuli. Nature. 435(7040):341–346.

Wehr M, Zador AM. 2003. Balanced inhibition underlies tuning and sharpens spike timing in auditory cortex. Nature. 426 (6965):442–446.

Weinberger NM, Bakin JS. 1998. Learning-induced physiological memory in adult primary auditory cortex: receptive fields plasticity, model, and mechanisms. Audiol Neurootol. 3(2-3):145–167.

Willmore B, Tolhurst DJ. 2001. Characterizing the sparseness of neural codes. Network. 12(3):255–270.

Wu GK, Tao HW, Zhang LI. 2011. From elementary synaptic circuits to information processing in primary auditory cortex. Neurosci Biobehav Rev. 35(10):2094–2104.

Xiong XR, Liang F, Li H, Mesik L, Zhang KK, Polley DB, Tao HW, Xiao Z, Zhang LI. 2013. Interaural level difference-dependent gain control and synaptic scaling underlying binaural computation. Neuron. 79(4):738–753.

Xiong XR, Liang F, Zingg B, Ji XY, Ibrahim LA, Tao HW, Zhang LI. 2015. Auditory cortex controls sound-driven innate defense behaviour through corticofugal projections to inferior colliculus. Nat Commun. 6:7224.

Xue M, Atallah BV, Scanziani M. 2014. Equalizing excitation–inhibition ratios across visual cortical neurons. Nature. 511 (7511):596–600.

Yazaki-Sugiyama Y, Kang S, Câteau H, Fukai T, Hensch TK. 2009. Bidirectional plasticity in fast-spiking GABA circuits by visual experience. Nature. 462(7270):218–221.

Yu Y, Migliore M, Hines ML, Shepherd GM. 2014. Sparse coding and lateral inhibition arising from balanced and unbalanced dendrodendritic excitation and inhibition. J Neurosci. 34(41): 13701–13713.

Zhang LI, Bao S, Merzenich MM. 2001. Persistent and specific influences of early acoustic environments on primary auditory cortex. Nat Neurosci. 4(11):1123–1130.

Zhang LI, Bao S, Merzenich MM. 2002. Disruption of primary auditory cortex by synchronous auditory inputs during a critical period. Proc Natl Acad Sci U S A. 99(4):2309–2314.

Zhang GW, Sun WJ, Zingg B, Shen L, He J, Xiong Y, Tao HW, Zhang LI. 2018. A non-canonical reticular-limbic central auditory pathway via medial septum contributes to fear conditioning. Neuron. 97(2):406–417.

Zhang LI, Tan AY, Schreiner CE, Merzenich MM. 2003. Topography and synaptic shaping of direction selectivity in primary auditory cortex. Nature. 424(6945):201–205.

Zhou M, Liang F, Xiong XR, Li L, Li H, Xiao Z, Tao HW, Zhang LI. 2014. Scaling down of balanced excitation and inhibition by active behavioral states in auditory cortex. Nat Neurosci. 17(6):841–850.